Published as *Physical Review A* **87**, 052515 (2013) on 28 May 2013

Smooth scaling of valence electronic properties in fullerenes: from one carbon atom, to C_{60}, to graphene

Greyson R. Lewis,[1] William E. Bunting,[1] Rajendra R. Zope,[2] Brett I. Dunlap,[3,*] and James C. Ellenbogen[1,†]

[1] *Nanosystems Group, The MITRE Corporation, McLean, VA, USA 22102*
[2] *Department of Physics, University of Texas at El Paso, El Paso, Texas 79958, USA*
[3] *Theoretical Chemistry Section, Code 6189, US Naval Research Laboratory, Washington, DC 20375, USA*

(Dated: May 22, 2013)

Scaling of quantum capacitances and valence electron detachment energies is studied for icosahedral and nonicosahedral fullerenes. Scaling trends are considered from zero to infinite average radius, where a fullerene's local surface properties are similar to those of graphene. Detailed density functional theory calculations are performed to determine the geometries and detachment energies of icosahedral fullerenes, while values of these quantities are obtained for nonicosahedral species from previously published experimental results. Strongly linear, quasiclassical scaling versus average radii $\overline{r}_n$ is seen for the quantum capacitances, but on two different scaling lines for icosahedral and nonicosahedral species, respectively. By contrast, nonclassical, nonlinear scaling versus $1/\overline{r}_n$ is seen for the electron detachment energies—i.e., the valence ionization potentials and electron affinities. This nonlinearity is not accounted for by classical theories that are used to explain trends in electronic properties of fullerenes and usually give accurate quantitative estimates. Instead, simple quantum equations are derived to account for nonlinearities in the metal-particle-like electron detachment energy scaling and to show that these are responsible for nonclassical, nonzero intercepts in the capacitance scaling lines of the fullerenes. Last, it is found that points representing the carbon atom and the graphene limit lie on scaling lines for icosahedral fullerenes, so their quantum capacitances and their detachment energies scale smoothly from one C atom, to C_{60}, to graphene.

I. INTRODUCTION

Fullerene molecules have fascinating and potentially valuable properties [1]. Because they are large molecules, though, containing many atoms and electrons, accurate quantum theoretical treatments are difficult and computationally intensive. Measurements of the electronic properties of the isolated molecules are similarly challenging [2, 3]. On the other hand, the regular, quasispherical structures of these pure carbon systems [4], along with results from quantum scaling investigations on other systems [5–8], suggest that the fullerenes' quantum properties, especially their valence energetics, might vary or "scale" with their dimensions in very regular ways. Understanding this quantum scaling, as well as how it differs from classically expected [9, 10] trends, might simplify greatly predictions of similar properties, even for very large fullerenes. Such insights also might provide an archetype for understanding and predicting such trends in the quantum electronic properties for homologous series of other large molecules or nanostructures. Still further, the structures of fullerenes permit us to envisage and to examine trends for a homologous series in which the smallest members are nanoscopic and, in principle, the largest could be truly macroscopic.

To those ends, here we explore the scaling of the fullerenes' quantum capacitances and valence electron detachment energies. The exploration follows the scaling trends, starting with a single carbon atom C_1 and continuing up to the limit of infinite average radius, where the local surface structure and geometry of a fullerene are very similar to that of graphene. These trends are followed for fullerenes of both icosahedral and nonicosahedral symmetries.

As seen in Fig. 1, two different, strongly linear, quasiclassical scaling trends are found for the icosahedral and nonicosahedral fullerenes, respectively, when their quantum capacitances [11, 12],

$$C_n = 1/(I_n - A_n), \tag{1}$$

are plotted versus their average radii $\overline{r}_n$. Above, I_n and A_n are the first ionization potential and first electron affinity, respectively, for an N-electron, n-carbon neutral fullerene C_n. These valence electron detachment energies are measured in eV, so values of quantum capacitances C_n are calculated in the molecular-scale units [5, 6] of fundamental positive charges per Volt ($+e$/V). Linear, symmetry-dependent scaling of C_n versus $\overline{r}_n$ for the fullerenes, as seen in Fig. 1, is similar to that observed previously for atoms [5, 8] and small molecules [6, 7].

In Figs. 2 and 3 it is observed, however, that the linear scaling behaviors of C_n versus $\overline{r}_n$ for the fullerenes are produced by values of I_n and A_n that each exhibit distinctly nonlinear scaling versus $1/\overline{r}_n$. In addition, these figures show that different types of nonlinearities are exhibited by the detachment energies of both the icosahedral and nonicosahedral species. Figure 2 further illustrates that such nonlinear behaviors are contrary to expectations (dotted lines) from purely classical theories [9, 10] that have been applied [3] to explain the scaling of fullerene detachment energies and their limiting

* brett.dunlap@nrl.navy.mil
† ellenbgn@mitre.org

behavior as $1/\overline{r}_n$ approaches zero.

At the same time, other nonclassical behaviors are seen in Fig. 1. These are the nonzero capacitance intercepts associated with the quantum capacitance scaling lines that otherwise are classical in form.

Moreover, it is discovered and proven algebraically in this work that the nonclassical, nonzero curvatures in the detachment energy trends for the fullerenes lead, via Eq. (1), to the nonclassical, nonzero intercepts in their otherwise classical capacitance scaling lines. These capacitance intercepts have two different signs for the icosahedral and nonicosahedral species, which correspond to the two different sets of curvatures for their detachment energy trends. This correspondence is summarized schematically in Fig. 4.

For the icosahedral fullerenes, the aforementioned results are derived from detailed density functional theory (DFT) calculations performed in this work to determine the valence electron detachment energies and average radii. We calculated I_n, A_n, and $\overline{r}_n$ for nine such molecules containing numbers of C atoms ranging from $n = 60$ to 2160. Also, for ten *non*icosahedral fullerenes of $\mathcal{C}_2$ and $\mathcal{D}_2$ symmetries, we tabulated from the literature experimental values [2, 3] of I_n and A_n, as well as theoretical values [13, 14] of $\overline{r}_n$. All these data, plus the associated values of C_n, appear in Table I and are used to plot the graphs in Figs. 1, 2, and 3.

II. METHOD AND RESULTS

To obtain the detachment energies for the nine icosahedral fullerenes, we performed DFT calculations, using a specially developed computer program [15]. The neutral-state geometry of each structure C_n was optimized and its average radius $\overline{r}_n$ determined using a Gaussian 6-311G** basis and a functional [16] that gives the experimental geometry for C_{60}. The DFT calculations involved the reoptimization of previously determined [17] icosahedral geometries, as well as the optimization of a new geometry for C_{320}. Unlike the other icosahedral fullerenes, which have closed-shell neutral ground states, C_{320} has an open-shell, triplet electronic state, with two unpaired electrons in the $33g_u$ orbital. This ionizes to a doublet cationic state, as do the other icosahedral fullerenes. After electron attachment, though, it does not yield the usual doublet, but forms a quartet anion with three electrons in the $33g_u$ orbital.

After determination of the neutral geometries, to evaluate the electron detachment energies, I_n=$[E_n(N-1)-E_n(N)]$ and A_n=$[E_n(N)-E_n(N+1)]$ for each n, the same program and basis, but a different functional that gives very accurate atomic energies [15], were used to separately determine the total energies, $E_n(N)$, $E_n(N-1)$, and $E_n(N+1)$, for the lowest-energy neutral, cationic and anionic states, respectively. Numerical results calculated in this way for the icosahedral fullerenes appear in part A of Table I.

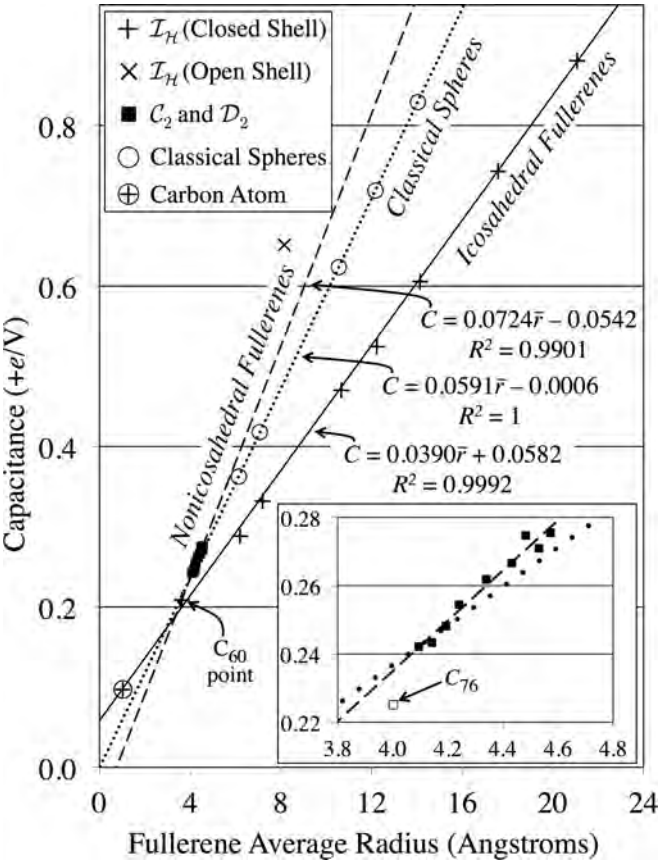

FIG. 1. Quantum capacitances C_n of n-carbon fullerenes plotted versus their average radii $\overline{r}_n$. The solid, dashed, and dotted regression lines, respectively, in the main portion of the figure, fit to high degree of confidence $(\overline{r}_n, C_n)$ points for icosahedral ($\mathcal{I}_h$) fullerenes (crosses), for *non*icosahedral fullerenes of $\mathcal{C}_2$ and $\mathcal{D}_2$ symmetries (dark squares), and for a classical sphere model (open circles) of the icosahedral fullerene capacitors. Regression equations and parameters for scaling lines are displayed in the graph. The inset expands the scale for the plot of the nonicosahedral fullerene points, their scaling line, and the classical scaling line. See text.

Part B of Table I presents the corresponding data for nonicosahedral fullerenes. These values were assembled from the experimental literature, as described in the previous section. Most of the experimental valence electron detachment energies available in the literature for nonicosahedral fullerenes were for species of $\mathcal{C}_2$ and $\mathcal{D}_2$ symmetries. Limited data [2, 3, 14] were available for species [1, 4] of other nonicosahedral symmetries, and these produced radius-capacitance points that were somewhat off the regression lines shown in the inset of Fig. 1 and in Fig. 3. However, the available data for points corresponding to species of these other symmetries were too sparse to determine scaling lines for them. Thus, we only display here the data and points for $\mathcal{C}_2$ and $\mathcal{D}_2$ nonicosahedral fullerenes.

The DFT I value and A value, 7.70 eV and 2.90 eV,

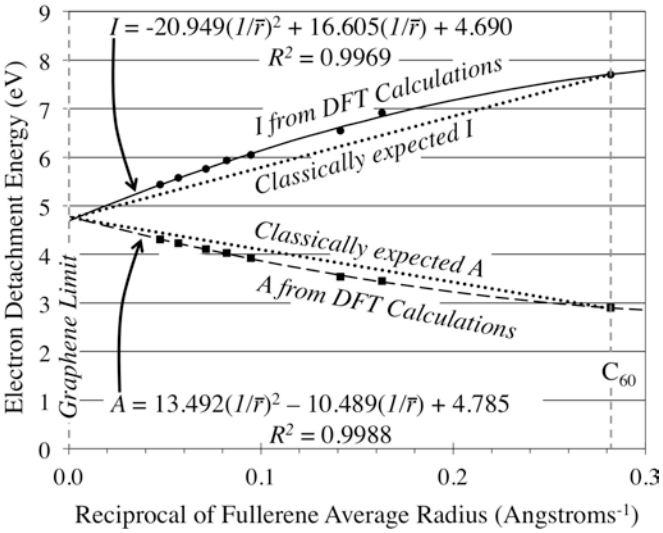

FIG. 2. Icosahedral fullerene ionization potentials (solid circles) and electron affinities (solid squares), as calculated in this work using density functional theory, are plotted versus reciprocals of the n-carbon neutral molecules' average radii, $1/\overline{r}_n$. Values are from part A of Table I. The solid, curved line for ionization potential function I and dashed, curved line for electron affinity function A are determined via second-order regression, for which equations and parameters appear in the figure. Dotted straight lines present scaling of I and A according to a purely classical electrostatic model. Points representing the carbon atom would lie on the solid and dashed lines for I and A, were the axes extended. See text.

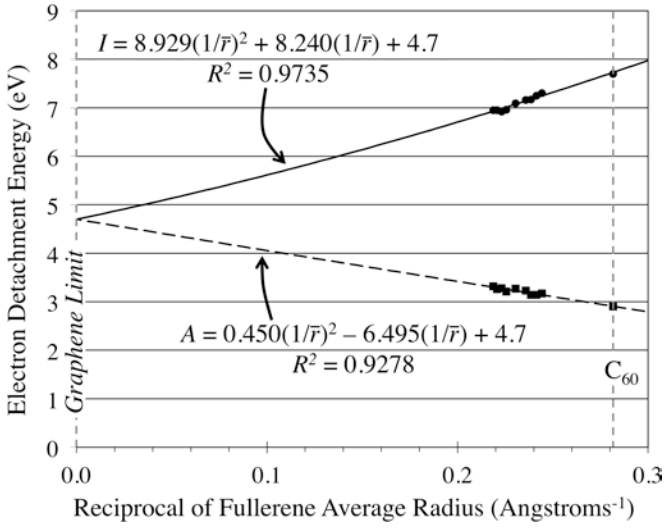

FIG. 3. Nonicosahedral fullerene ionization potentials (solid circles) and electron affinities (solid squares) are plotted versus reciprocals of the n-carbon neutral molecules' average radii, $1/\overline{r}_n$. Values of I_n and A_n are from experimental results reported in the literature and presented in part B of Table I. Values of $1/\overline{r}_n$ are from theory [13, 14]. As in Fig. 2, the solid, curved line for ionization potential function I and dashed, curved line for electron affinity function A are determined via second-order regression, for which equations and parameters appear in the figure. Unlike the nonlinear regression lines in Fig. 2, above, the lines' intercepts at $(1/\overline{r}_n) = 0$ were fixed in advance at the value of the graphene work function, 4.7 eV. See text.

respectively, that are calculated for C_{60} and presented in part A of Table I each are in reasonably good agreement with the respective experimental values [2, 3] of 7.57 eV and 2.65 eV. The relative errors of 1.7 and 9.4 per cent differ considerably, but the absolute errors of concern in calculating the capacitance via Eq. (1) are small, of the same sign, and of approximately the same magnitude. Thus, they nearly cancel in calculating C_{60}. For this reason, we have seen that substituting a value of C_{60} determined from the experimental I and A values affects the capacitance scaling parameters very little, though it makes the already high R^2 value very slightly higher.

The source of the small absolute errors in the C_{60} detachment energies is believed to arise primarily from the self-interaction in the DFT local-density approximation. This self-interaction might be removed, but only with considerable computational cost. Using a different density functional, the effect of the self-interaction was studied for atoms and small, well-behaved molecules [20]. It was found that the self-interaction error in the detachment energies decreased as the number of electrons increased. If that is the case here, the effect on the capacitance scaling of not correcting I and A for the self-interaction should be negligible. However, even if self-interaction errors like those seen in C_{60} were to persist in I and A for the larger fullerenes, they would be expected to cancel each other, for the most part, in calculating the capacitances via Eq. (1). To be sure of the DFT-based scaling trends, though, we replotted the capacitance scaling line for the icosahedral fullerenes assuming the same percentage errors in I and A for the larger molecules as for C_{60}. Then, we replotted again assuming the same absolute errors in I and A as for C_{60}. In both of these sensitivity analyses the effects on the capacitance scaling were very small: the linear scaling trend remained very strong, with no diminishment in the R^2 values, and the regression lines still passed through the point for the carbon atom.

In Fig. 1, the solid line and the dashed line in the large graph are fit by linear regression to the icosahedral and nonicosahedral $(\overline{r}_n, C_n)$ points from parts A and B, respectively, of Table I. The inset within the figure provides a more detailed view of the nonicosahedral capacitance scaling line and the points that define it, all of which represent fullerenes of $\mathcal{C}_2$ or $\mathcal{D}_2$ symmetry types, as indicated in the table. Each $(\overline{r}_n, C_n)$ point on the nonicosahedral scaling line represents values associated with the lowest energy [18, 19] neutral geometry for that value of n.

In the inset of Fig. 1, it also is seen that the radius-capacitance point for C_{76} (open square) falls significantly below the scaling line. This is because the experimental

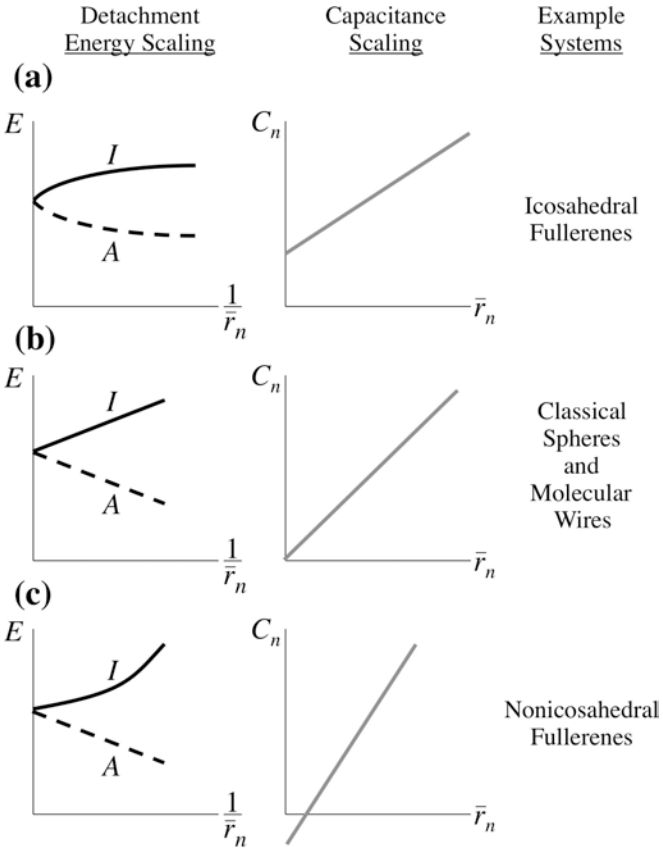

FIG. 4. Sketches for three basic cases, (a)-(c), illustrating the relationship between the scaling versus $1/\overline{r}_n$ of the electron detachment energies I and A (depicted at left) and the scaling versus $\overline{r}_n$ of the quantum capacitances C_n derived from those detachment energies (depicted at right). Specifically, the sketches show the manner in which the intrinsic nonlinearities seen in the quantum electron detachment energy graphs at left in parts (a) and (c) of the figure, as well as in Figs. 2 and 3, are associated with the nonclassical, nonzero intercepts shown in the corresponding capacitance graphs at right, as well as in Fig. 1. By contrast, as shown in part (b) above, purely classical linear scaling of the detachment energies leads the capacitance intercept to vanish. Classical scaling is not realized for the fullerenes, but is a very good approximation for molecular wires [6]. See text.

value determined by Boltalina *et al.* for A_{76} does not conform to the trend of increasing value with fullerene size that those investigators observed for other fullerene electron affinities [2]. The discrepancy in this A value is significant enough that the experimentalists remark upon it in their paper. For this reason, we did not use points for the C_{76} molecule in any of the regressions in this work. However, we include the C_{76} point in Fig. 1 for completeness, along with points for the other fullerenes of $\mathcal{C}_2$ or $\mathcal{D}_2$ symmetry for which detachment energies were measured [2, 3] by Boltalina *et al.*

Additionally, because the values of I_n and $\overline{r}_n$ for C_{76} that appear in Table I are thought to be accurate, we can apply the nonicosahedral fullerene capacitance scaling parameters shown in Fig. 1 to provide an improved estimate [7, 8] for the electron affinity, $A_{76} = 3.08$ eV. This estimate is improved in the sense that it would place the radius-capacitance point for C_{76} on the scaling line

TABLE I. Quantum capacitances C_n for n-carbon fullerenes tabulated as a function of their average radii $\overline{r}_n$. Values of C_n are calculated via Eq. (1) from each fullerene's ionization potential I_n and electron affinity A_n. In part A of the table, I_n and A_n are determined for icosahedral fullerenes via detailed density functional theory calculations performed in this work, while in part B they are from experiments on *non*icosahedral fullerenes by Boltalina *et al.* [2, 3]. Data are tabulated here only for nonicosahedral fullerenes of $\mathcal{C}_2$ and $\mathcal{D}_2$ symmetries. See text.

Number of Carbon Atoms, n	Average Radius[a], $\overline{r}_n$ (Å)	Ionization Potl., I_n (eV)	Electron Affinity, A_n (eV)	Quantum Capacitance from Eq. (1) [b], C_n ($+e$/V)	Symmetry[c]
A. Icosahedral Fullerenes					
60	3.548	7.6996	2.9005	0.2084	$\mathcal{I}_h$
180	6.135	6.9189	3.4520	0.2884	$\mathcal{I}_h$
240	7.073	6.5460	3.5379	0.3324	$\mathcal{I}_h$
320[d]	8.038	5.7332	4.1975	0.6512	$\mathcal{I}_h$
540	10.553	6.0483	3.9212	0.4701	$\mathcal{I}_h$
720	12.166	5.9342	4.0278	0.5245	$\mathcal{I}_h$
960	14.034	5.7617	4.1097	0.6053	$\mathcal{I}_h$
1500	17.522	5.5736	4.2276	0.7430	$\mathcal{I}_h$
2160	21.014	5.4419	4.3068	0.8810	$\mathcal{I}_h$
B. Nonicosahedral Fullerenes					
76[e]	3.991	7.34	2.89	0.238	$\mathcal{D}_2$
80	4.094	7.30	3.17	0.242	$\mathcal{D}_2$
82	4.142	7.25	3.14	0.243	$\mathcal{C}_2$
84	4.193	7.17	3.14	0.248	$\mathcal{D}_2$
86	4.241	7.16	3.23	0.254	$\mathcal{C}_2$
90	4.339	7.09	3.27	0.262	$\mathcal{C}_2$
94	4.432	6.96	3.21	0.267	$\mathcal{C}_2$
96	4.482	6.92	3.28	0.275	$\mathcal{D}_2$
98	4.53	6.95	3.26	0.271	$\mathcal{C}_2$
100	4.572	6.95	3.32	0.275	$\mathcal{D}_2$

[a] Average radius $\overline{r}_n$ is the arithmetic mean of distances of all the carbon atoms in a fullerene from a central point within the molecule, as determined from icosahedral fullerene geometries optimized in this work and from nonicosahedral geometries due to Yoshida and Osawa [13, 14].

[b] Quantum capacitances C_n are reported in $+e$/V, fundamental units of positive charge per Volt. Multiplication by 1.602188×10^{-19} Coulombs per fundamental unit of charge converts these capacitances to the more familiar mks units of Farads. Using these capacitance units, the permittivity of free space is $\epsilon_0 = 5.526350 \times 10^{-3}$ $+e$/V-Å.

[c] For nonicosahedral fullerenes, symmetry type is taken from Shao *et al.* [18, 19] for the lowest energy fullerene with that number of carbon atoms.

[d] C_{320} has an open-shell electronic structure, unlike that of the other icosahedral fullerenes listed, which are closed shell.

[e] C_{76} point not used in regressions. A better estimate for the species' electron affinity might be $A_{76} = 3.08$ eV. See text.

with those of the other nonicosahedral fullerenes.

The linear fits that define the icosahedral and nonicosahedral capacitance scaling lines both are very strong, as seen from the large values of R^2 for each displayed in Fig. 1. Additionally, it is seen there that the icosahedral and nonicosahedral scaling lines nearly intersect at the C_{60} point. This might be explained by observing that C_{60} is a kind of "progenitor" structure for both symmetry types, because it is the only fullerene whose points all rest on a single sphere. As more carbon atoms are added to produce larger fullerenes, two growth paths are possible: either the carbons are added in such a way as to maintain the high-symmetry, truncated icosahedral structure of C_{60}, or they are added in such a way as to reduce the symmetry of the molecule.

We observe further in Fig. 1 that the radius-capacitance point for the C atom [5] lies right on the scaling line defined by the $(\overline{r}_n, C_n)$ points for the icosahedral fullerenes, even though the C atom point is not used in the regression that determines the line. If the C atom point were to be included in the regression with the points for the icosahedral fullerenes, though, the correlation coefficient would *increase* to $R^2 = 0.9994$. For this reason, the carbon atom may be thought of as a progenitor capacitive structure for the icosahedral fullerene capacitors; the icosahedral molecules share a certain similarity to the atom in their valence energetics.

The regression lines in Fig. 1 have equations of the form

$$C = 4\pi\epsilon_0\kappa\overline{r} + C_0, \tag{2}$$

where $\epsilon_0 = 5.526350 \times 10^{-3}$ $+e/\text{V}-$ Å is the permittivity of free space. The first term on the right of Eq. (2) is Faraday's and Maxwell's law for spherical capacitors in classical electrostatics [21, 22]. Thus, the dimensionless parameter κ, which determines the slope of the scaling line, is the analog of a classical dielectric constant, but for individual fullerene molecules. Equation (2) implies the values 0.562 and 1.043 for κ in the icosahedral and nonicosahedral cases, respectively. A strikingly nonclassical [5] feature, though, is the additional constant term C_0 that is required to account for the empirically observed nonzero values of the capacitance intercepts at $\overline{r} = 0$.

In Fig. 2, the icosahedral fullerenes' electron detachment energies from part A of the table are plotted versus the reciprocal of the icosahedral fullerenes' average radii. Then, two second-order fits determine the regression curves through the $(1/\overline{r}_n, I_n)$ and $(1/\overline{r}_n, A_n)$ points, respectively. The values of I_n and A_n are seen to progress smoothly along these curves, from those for C_{60} at the far right to very nearly equal intercepts $I_\infty \approx A_\infty \approx 4.7$ eV at $1/\overline{r}_n = 0$ (the limit of very large, macroscopic fullerenes). There, the energy gap $(I_n - A_n)$ vanishes to the accuracy of the calculations. Such an intercept sometimes is taken to be an estimator for the work function of graphene [3], which the carbon surface of a very large fullerene locally resembles. This is because, in the limit of very large n and $\overline{r}_n$, a fullerene's surface is effectively flat, locally, and consists of almost purely hexagonal arrangements of atoms, since it still contains only a small, fixed number of pentagonal "impurities" (12 for any fullerene). The limiting value of 4.7 eV determined here is in close agreement with prior estimates of 4.6 eV for the work function of graphene [23] and graphite [24], which are thought to be approximately equal.

Figure 3 analogously plots data from part B of Table I for the nonicosahedral fullerenes. A difference in the fitting procedure for Fig. 3, though, is that we fixed the intercepts with the energy axis at the value of the work function of graphene: $I_\infty = A_\infty = 4.7$ eV. Then, we performed the regression analyses to determine the curves.

The curves in Figs. 2 and 3 are fit with high confidence to the points via second-order regression, defining polynomial expansions:

$$I_n = I_\infty + \lambda_I(1/\overline{r}_n) + \frac{1}{2}\tau_I(1/\overline{r}_n)^2 \tag{3a}$$

$$A_n = A_\infty + \lambda_A(1/\overline{r}_n) + \frac{1}{2}\tau_A(1/\overline{r}_n)^2. \tag{3b}$$

Parameters λ_k and τ_k represent the slopes and curvatures, respectively, of the detachment energy scaling curves. The fact that the progression of the detachment energies from those of C_{60} to the limiting values, I_∞ and A_∞, occurs along second-order, curved functions of $1/\overline{r}$ contrasts with the linear functions of $1/\overline{r}$ anticipated by simple, classical electrostatic models [9, 10], as noted above.

Such linear functions are displayed in Fig. 2 as the dotted lines that were constructed to connect the I_{60} point and the A_{60} point to I_∞ and A_∞, respectively. It is seen that these classical lines give reasonable approximations for all the I and A values determined by DFT for the icosahedral fullerenes. A similarly constructed classical linear approximation would be even closer to the solid and dashed scaling curves shown in Fig. 3 for the nonicosahedral fullerene detachment energies. In fact, the dotted lines are not drawn in for the classical approximation because they would be too close to the curves determined by the experimental values, and would obscure them.

The classically expected lines in Fig. 2 have the equations I=10.642$(1/\overline{r})$+4.7 and A=−6.385$(1/\overline{r})$+4.7. Values of I_n and A_n from along these classically expected detachment energy functions are used to determine the classically expected capacitances for each $\overline{r} = \overline{r}_n$, and thereby plot the points (open circles) and their dotted classical capacitance regression line in Fig. 1, which has an intercept C_0 that vanishes to the accuracy of the data.

By definition, the dotted classical capacitance regression line in Fig. 1 goes through the radius-capacitance point for C_{60}. Even so, it is seen that it does not give good estimates for the capacitances of the other icosahedral fullerenes (along the solid regression line). However, the dotted classical line provides good quantitative estimates for the capacitances of the nonicosahedral fullerenes (along the dashed regression line). This

is made particularly clear by the close proximity of the two scaling lines in the inset of the figure.

In order to preserve the detail presently seen in Fig. 2, the points for a single carbon atom are not included on the graph there. Nonetheless, just as the point representing the carbon atom or C_1 lies on the quantum capacitance scaling line for the icosahedral fullerenes in Fig. 1, the points representing C_1 (with $1/\overline{r}_1 = 1.087$ Å^{-1}, $I = 11.26$ eV, and $A = 1.26$ eV) would be seen to lie on the icosahedral fullerene quantum scaling curves for I and A in Fig. 2, were the scales of the axes extended. Inclusion of these C_1 points in the regressions does induce a small energy gap of approximately 0.3 eV between I and A in the plot at $1/\overline{r} = 0$. However, fits versus $1/\overline{r}$ of fullerene detachment energies, including the C_1 points, both are very strong, with $R^2 = 0.997$ for both I and A. Further, if the induced gap is eliminated from these fits, by constraining both intercepts at $1/\overline{r} = 0$ to assume the value of the graphene work function, 4.7 eV, the fits continue to be very strong, with $R^2 \geq 0.992$ for both curves. Thus, an additional important result of this work is that both the quantum capacitances and the electron detachment energies of icosahedral fullerenes scale smoothly from the limit of a single carbon atom, through points for C_{60}, to the points representing a graphene-like structure, in the limit of $n = \infty$ at $1/\overline{r} = 0$.

III. DISCUSSION AND ANALYSIS

Analysis of the foregoing results reveals that the nonzero quantum capacitance intercepts C_0 for the fullerenes, as seen in Fig. 1, are a consequence of the nonclassical, nonlinear scaling of the electron detachment energy functions in Figs. 2 and 3, and *vice versa*. To demonstrate this algebraically, we substitute Eqs. (3) in Eq. (1), then expand the result in a geometric series through first order in $\overline{r}_n$:

$$C_n = \Big(\frac{1}{\lambda_I - \lambda_A}\Big)\overline{r}_n + \frac{1}{2}\Big[\frac{\tau_A - \tau_I}{(\lambda_I - \lambda_A)^2}\Big]. \qquad (4)$$

To derive this result, we assume that $I_\infty \approx A_\infty$, so that their difference vanishes, at least approximately, as discussed above. Then, order-by-order comparison of Eq. (4) to Eq. (2) enables us to evaluate in terms of the slope and curvature of the detachment energy scaling curves the molecular dielectric constant

$$\kappa = \frac{1}{4\pi\epsilon_0}\Big(\frac{1}{\lambda_I - \lambda_A}\Big) \qquad (5)$$

and the capacitance intercept

$$C_0 = \frac{1}{2}\Big[\frac{\tau_A - \tau_I}{(\lambda_I - \lambda_A)^2}\Big] \qquad (6a)$$

$$= 8\pi^2\epsilon_0^2\kappa^2(\tau_A - \tau_I). \qquad (6b)$$

Equations (4) through (6) involve no classical approximations.

Now, applying Eq. (6b) to Fig. 2, for example, it is seen that the curvatures, τ_A and τ_I, of the second-order regression curves for I_n and A_n are of opposite sign, so the two curvatures do not cancel in Eq. (6b) and C_0 does not vanish. Thus, from Eq. (6b), the positive nonzero capacitance intercept may be regarded as a consequence of the nonzero curvatures of the detachment energy scaling curves plotted in Fig. 2. This case also is summarized in Fig. 4(a).

Evaluating Eq. (6b) for the case depicted in Fig. 3 once again yields a nonzero value of C_0. Here, however, the difference between the curvatures is negative because $\tau_I > 0$ and $\tau_A \approx 0$. Thus, $C_0 < 0$, as plotted in Fig. 1 and depicted schematically in Fig. 4(c).

Conversely, we also may regard the nonzero curvatures for the detachment energy graphs as a consequence of a nonzero capacitance intercept. Considering only the valence ionization potential and starting from the purely classical electrostatic formulas of Smith [9] and of Leach [10], we may write:

$$I_n = I_\infty + 1/2C_n \qquad (7a)$$

$$\approx I_\infty + \Big(\frac{1}{8\pi\epsilon_0\kappa}\Big)\frac{1}{\overline{r}_n} - 2C_0\Big(\frac{1}{8\pi\epsilon_0\kappa}\Big)^2\Big(\frac{1}{\overline{r}_n}\Big)^2. \qquad (7b)$$

The second line in the previous equation follows from substitution of quantum capacitance equation (2) into Eq. (7a), then applying a first-order geometric series expansion to the result. Analogously, using Smith's [9] classical expression for the electron affinity as a starting point, we may write:

$$A_n = A_\infty - 1/2C_n \qquad (8a)$$

$$\approx A_\infty - \Big(\frac{1}{8\pi\epsilon_0\kappa}\Big)\frac{1}{\overline{r}_n} + 2C_0\Big(\frac{1}{8\pi\epsilon_0\kappa}\Big)^2\Big(\frac{1}{\overline{r}_n}\Big)^2. \qquad (8b)$$

In Eqs. (7) and in Eqs. (8), to obtain the third term on the right that corresponds to a nonzero curvature like that observed in the quantum results plotted in Fig. 2, it is essential that the expansions above utilize *both* terms of Eq. (2). This differs from the purely classical expansion procedure employed by Smith [9] and by Leach [10] that utilizes only the first term on the right of Eq. (2), effectively setting $C_0 = 0$ in Eqs. (7b) and (8b).

The expressions in Eq. (7b) and Eq. (8b) for the coefficients of the powers of $1/\overline{r}_n$ can be verified to be reasonably accurate, quantitatively. For example, we obtain from the regression equations in Fig. 1 the values $4\pi\epsilon_0\kappa = 4.69\ +e$/V-Å and $C_0 = 0.0582\ +e$/V, in the case of the icosahedral fullerenes. Using these in Eq. (7b), the values for the first and second-order coefficients are 12.82 eV-Å and -19.13 eV-Å^2, respectively. These compare favorably to the respective values 16.61 eV-Å and -20.95 eV-Å^2 seen in the regression equation for the accurate ionization potentials in Fig. 2.

Continuing the derivation, from a comparison of Eqs. (7b) and (8b) with Eqs. (3a) and (3b), respectively, one may obtain approximate relations for the slopes and

curvatures of I and A with respect to $1/\overline{r}$:

$$\lambda_I = -\lambda_A = \frac{1}{8\pi\epsilon_0\kappa} \tag{9}$$

$$\tau_I = -\tau_A = -4C_0\lambda_I^2. \tag{10}$$

Equations (7b) through (10) incorporate quantum effects in the nonzero curvatures, but can only be approximate because of the use of the classical expressions in Eqs. (7a) and (8a) as starting points in their derivations. Nonetheless, Eqs. (9) and (10), along with Eq. (3), do provide a rationale for the near symmetry of I and A as a function of $1/\overline{r}$ that is manifest in both Fig. 2 and Fig. 3.

From the accurate quantum results embodied in the regression equations within these figures one can verify, as well, that $\tau_I \approx -\tau_A$. In the values of the regression parameters for the icosahedral fullerenes given in Fig. 2, there is order of magnitude agreement of τ_I and τ_A with Eq. (10). In Fig. 3, for the nonicosahedral fullerenes, the approximate agreement with this curvature relation is manifest if one recognizes there that $\tau_A \approx 0$.

Equation (10) also shows explicitly that a nonzero capacitance intercept results in a nonzero curvature for I and for A as a function of $1/\overline{r}_n$, as asserted above. Still further, from that equation it is clear that the *sign* of the capacitance intercept C_0 and the signs of the curvatures τ of the detachment energy scaling graphs are mutually related. Thus, for example, just as a positive value of C_0 for the icosahedral fullerenes is ensured by (and ensures) a negative value of τ_I, a negative value of C_0 in the case of the nonicosahedral fullerenes is associated with a positive value of τ_I. This can be verified empirically from the results in Figs. 1, 2, and 3.

More generally, in Fig. 4, we map out schematically three major cases of this relationship between the quantum capacitance intercepts and the curvatures in detachment energy scaling graphs. These apply for the fullerenes studied here and for molecular wires studied in prior work [6]. Other cases may arise for still other quantum systems. For the cases depicted in Figs. 2, 3, and 4, the near symmetry in the scaling of I and A about the work function in the fullerenes strongly resembles that observed previously for clusters of metal atoms [12, 25] and affirms the fullerenes' classification as semimetals.

Considering the results displayed in Fig. 1 from a more qualitative viewpoint, the two different scaling lines for the differently shaped icosahedral and nonicosahedral fullerenes, respectively, are consistent with the classical notion that capacitances depend strongly on the shapes of capacitors. In this connection, we observe further that the nonicosahedral fullerene capacitances lie above the scaling line for the icosahedral fullerenes. This is consistent with the facts that (a) isoperimetric principles [26] of classical electrostatics indicate that the capacitance of a conductor of any shape is proportional to the square root of its surface area, and (b) the more aspherical nonicosahedral species should have larger surface areas for a given average radius than do icosahedral fullerenes.

In addition, we see in Fig. 1 that the radius-capacitance point for open-shell C_{320} (the $\times$) lies well above the scaling line for the other icosahedral fullerenes, which have closed-shell valence electron configurations. This outlier point suggests that electronic structure (esp., the multiplicity), as well as the geometric structure of the nuclear framework, plays an important role in determining the effective shape and dimensions of a fullerene capacitor. A related explanation of the inordinately large capacitance of C_{320} is that its open-shell electronic structure is more diffuse. This produces a larger effective radius and surface area of its valence electron distribution for its value of $\overline{r}_n$ than would a closed-shell electron distribution.

IV. SUMMARY AND CONCLUSIONS

In summary, we have studied the scaling of fullerene quantum capacitances as a function of their average radii $\overline{r}_n$ and the scaling of the molecules' valence electron detachment energies as a function of $1/\overline{r}_n$. Detailed density functional theory calculations of electron detachment energies for icosahedral fullerenes and results from earlier experimental measurements of detachment energies for nonicosahedral fullerenes were employed for this purpose. Linear scaling was found for the capacitances of both symmetry types; however, this scaling occurred along two different scaling lines, one for icosahedral fullerenes and one for nonicosahedral fullerenes of $\mathcal{D}_2$ and $\mathcal{C}_2$ symmetries. (See Fig. 1.)

Though linear scaling was found for the capacitances as a function of $\overline{r}_n$, nonclassical, *non*linear scaling was found for the fullerene detachment energies as a function of $1/\overline{r}_n$. These nonlinear trends were seen to resemble those for clusters of metal atoms. Further, a proof in Section III shows that the nonlinear behavior seen in Figs. 2 and 3 for the detachment energies leads to the nonclassical, nonzero intercepts seen in Fig. 1 for the capacitance scaling lines. The converse also was proven to be true.

Thus, classical scaling is not realized in the fullerenes. Classical models [9, 10] commonly employed to represent their detachment energies and capacitances yield reasonably good quantitative estimates, but fail to reproduce key features of the accurate quantum scaling trends. Especially, they miss the nonlinearity of the detachment energies as a function of $1/\overline{r}_n$ and nonzero intercepts for the capacitance as a function of $\overline{r}_n$. They also fail to account for the differences between the trends for the icosahedral and nonicosahedral species. Instead, a simple set of algebraic equations is derived in Section III to explain these quantum behaviors and the relationships among them, as well as to contrast them with classically expected behaviors.

Quantum capacitance scaling of the icosahedral and nonicosahedral fullerenes also is contrasted with classically expected capacitance scaling in Fig. 1, while the departures from classical detachment energy scaling are shown in Figs. 2 and 3. The relationships discovered be-

tween the nonclassical detachment energy scaling behaviors and the nonclassical features in quantum capacitance scaling are depicted conceptually in Fig. 4.

Another key finding of this work is that points representing the carbon atom lie on scaling lines for icosahedral fullerenes, as do points for C_{60}, while the detachment energy scaling curves also intersect points representing a graphene-like structure in the limit of very large radius. Thus, the icosahedral fullerene quantum capacitances and electron detachment energies all scale smoothly from a single carbon atom to the graphene limit.

Last, the algebraic formalism derived to show the connection between nonclassical behaviors in detachment energy scaling and quantum capacitance scaling for fullerenes should be useful, as well, for interpreting quantum scaling trends for other systems, such as atoms [5] and diatomic molecules [7]. Similarly, the equations and conceptual insights developed here may be useful in providing more accurate, simple estimators of electron detachment energies for other homologous series of molecules and for still other types of nanostructures.

ACKNOWLEDGMENTS

The authors gratefully acknowledge valuable conversations with C. Picconatto and S. Das of the MITRE Nanosystems Group, plus valuable comments on the manuscript by C. White of NRL. At MITRE, this research was funded by the MITRE Innovation Program, while at the Naval Research Laboratory it was supported by the Office of Naval Research, both directly and through NRL. At UT-El Paso, financial support came from DOE Basic Energy Sciences Grant DE-SC0006818.

[1] M. S. Dresselhaus, G. Dresselhaus, and P. C. Eklund, *Science of Fullerenes and Carbon Nanotubes* (Academic Press, San Diego, CA, 1996)
[2] O. V. Boltalina, E. V. Dashkova, and L. N. Sidorov, Chem. Phys. Lett. **256**, 253 (1996)
[3] O. V. Boltalina, I. N. Ioffe, L. N. Sidorov, G. Seifert, and K. Vietze, J. Am. Chem. Soc. **122**, 9745 (2000)
[4] P. W. Fowler and D. E. Manolopoulos, *An Atlas of Fullerenes* (Dover, New York, 2006)
[5] J. C. Ellenbogen, Phys. Rev. A **74**, 034501 (2006)
[6] J. C. Ellenbogen, C. A. Picconatto and J. S. Burnim, Phys. Rev. A **75**, 042102 (2007)
[7] J. C. Ellenbogen, Phys. Rev. A **82**, 012508 (2010)
[8] W. E. Bunting and J. C. Ellenbogen, Phys. Rev. A **85**, 062503 (2012)
[9] F. T. Smith, J. Chem. Phys. **34**, 793 (1960)
[10] S. Leach, Can. J. Phys. **79**, 501 (2001)
[11] G. J. Iafrate, K. Hess, J. B. Krieger, and M. Macucci, Phys. Rev. B **52**, 10737 (1995)
[12] J. P. Perdew, Phys. Rev. B **37**, 6175 (1988)
[13] M. Yoshida and E. Osawa, Fullerenes, Nanotubes and Carbon Nanostructures **1**, 55 (1993)
[14] S. Weber, "VRML gallery of fullerenes," http://jcrystal.com/steffenweber/gallery/Fullerenes/Fullerenes.html (1999). This Web site provides a database of M.Yoshida's optimized coordinate files for fullerene structures.
[15] R. R. Zope and B. I. Dunlap, Phys. Rev. B **71**, 193104 (2005)
[16] B. I. Dunlap and R. R. Zope, Chem. Phys. Lett. **422**, 451 (2006)
[17] R. R. Zope, T. Baruah, M. R. Pederson, and B. I. Dunlap, Phys. Rev. B **77**, 115452 (2008)
[18] N. Shao, Y. Gao, S. Yoo, W. An, and X. C. Zeng, J. Phys. Chem. **110**, 7672 (2006)
[19] N. Shao, Y. Gao, and X. C. Zeng, J. Phys. Chem. C **111**, 17671 (2007)
[20] O. A. Vydrov and G. E. Scuseria, J. Phys. Chem. **122**, 184107 (2005)
[21] D. Halliday, R. Resnick, and J. Walker, *Fundamentals of Physics*, sixth ed. (Wiley, New York, NY, 2001)
[22] J. C. Maxwell, *A Treatise on Electricity and Magnetism*, Vol. 1 (Clarendon Press, Oxford, England, 1873). See esp. pp. 219-221. Available online at URL: http://posner.library.cmu.edu/Posner/books/book.cgi?call=537_M46T_1873_VOL._1
[23] Y.-J. Yu, Y.Zhao, S. Ryu, L. Brus, K. S. Kim, and P. Kim, Nano Lett. **9**, 3430 (2009)
[24] J. Chen, W. Wang, M. A. Reed, A. M. Rawlett, D. W. Price, and J. M. Tour, Appl. Phys. Lett. **76**, 4007 (2000)
[25] M. Seidl, K. H. Meiwes-Broer, and M. Brack, J. Chem. Phys **95**, 1295 (1991)
[26] G. Polya and G. Szegö, *Isoperimetric Inequalities in Mathematical Physics*, Annals of Mathematics Studies No. 27 (Princeton Univ. Press, Princeton, NJ, 1951)